Characterization of Heat Transfer in Serpentine Passages using Thermochromic Liquid Crystals

Undergraduate Thesis

By:

Aditya Narayan Kulkarni

The Ohio State University

2018

Advisor:

Dr. Randall Mathison

Committee: Dr. Randall Mathison

Dr. Michael Dunn

Contents

Table of Figures

Abstract

Since the beginning of the 21st century, air travel has increased over 120%, creating a need for more efficient propulsion. Recent innovations in aircraft gas turbine technology have centered around cold section improvements such as geared fans and higher-pressure ratio compressors. However, improvements in the thermodynamic cycle of the engine that push turbine inlet temperatures ever higher remain an instrumental part in improving efficiency for future aircraft. At the Gas Turbine Laboratory (GTL), experiments using engine hardware are performed at scaled conditions to provide a better understanding of the flow physics and heat transfer in the high-pressure turbine section. The GTL has completed experiments utilizing enlarged versions of turbine blade serpentine passages employing the industry accepted isothermal copper panel method and the newer thermochromic liquid crystal (TLC) method. TLCs change color as they are exposed to a range of temperatures, and the heat transfer is derived from the rate of temperature change. Measurements with TLCs offer an advantage in that they are a 2-dimensional technique that result in a detailed map of heat transfer across the passage. This provides designers with the detailed data required to improve passage design. However, there is less confidence in the measurements from TLCs. This project proposes a new route to verify the solutions from the TLCs and correlate them to copper panel experiments. Previous work on this project centered around heat transfer algorithm verification and post-processing of full-scale rotating test section data. This research expands upon previous work by performing simplified single panel experiments using warm-band TLCs. The advantage of this project is the elimination of many variables present in the more complicated rotating experiment: fisheye distortion, glares, and inaccurate calibration of TLCs. This will be accomplished by a reduction in scale and measuring temperatures with infrared cameras to provide accurate in-situ calibrations. The results from this experiment will be compared to other small-scale copper panel experiments, the effects of turbulators will be analyzed in more detail, and further progress on calibration and post processing will be demonstrated.

Acknowledgements

Firstly, I would like to thank Dr. Mathison for his guidance on this research project and over the past 3 years in general. Without his guidance, none of the work completed over the past 3 years would have been possible nor would I have found my passion for conducting research and pursuing a graduate education. I would also like to thank all the graduate students and staff at the Gas Turbine Laboratory for their assistance over the past 3 years and for keeping me entertained with their humor. Additionally, I appreciate and thank the College of Engineering for the research scholarship bestowed upon me. Lastly, I would like to thank my family and friends for their support.

Chapter 1: Introduction

This chapter provides an introduction to the field of gas turbine cooling and why it is so essential to increase efficiency. The chapter provides a brief literature review on the copper panel experiment completed at The Ohio State University Gas Turbine Laboratory (GTL) and other techniques and experiments completed using thermochromic liquid crystals (TLCs).

1.1 Introduction

Global reliance on gas turbine engines has increased exponentially since the early 1990s and so has the need for higher efficiency engines. To produce a more efficient engine, industry has focused its efforts on higher pressure ratio compressors, variable pitch fans, geared fans, and improved cooling techniques. At the Gas Turbine Laboratory (GTL), experiments are conducted on film cooling and internal cooling using different techniques to examine the flow physics in passages and greatly improve accuracy and resolution of predicted heat transfer. This project focuses on heat transfer using thermochromic liquid crystals (TLCs) and its application to internal serpentine passages on high pressure turbine blades. Previously, the GTL conducted isothermal copper panel experiments on serpentine passages to attempt to match the NASA HOt Section Technology (HOST) data (Smith, Mathison, & Dunn, 2013). Data from the isothermal experiment correlated well with NASA host data, and there was strong interest in obtaining more detailed measurements utilizing TLCs if they could be validated against NASA's results.

After the completion of the isothermal copper panel experiments, Lawler began experiments using TLCs painted onto a stationary serpentine passage with aspect ratio of one (Lawler, 2015). These experiments are different from the previous cases because the wall temperature is transient. TLCs are crystals whose molecules rotate when exposed to different temperatures, and this rotation gives off varying hue values. The TLC is limited to an "active range" where the molecules will show color, and outside the active range, the molecules will turn clear and the black paint behind the TLC will be visible to the camera. The advantage of TLCs is the ability to view heat transfer results with increased spatial

resolution. In isothermal experiments, a 2-inch long panel is area-averaged and averaged over time to find a local Nusselt number. Results from multiple panels can and then be plotted together across the span of the passage. In contrast, local heat transfer rates can be determined for any location in the passage from TLCs. However, Lawler's Nusselt numbers deviated from the data presented by NASA. After the completion of Lawler's stationary TLC experiments, the GTL built a facility to conduct experiments on rotating serpentine passages. A picture of the facility in the spin-pit is seen in Figure 1. Similar to Lawler's experiments, the full scale rotating test section exhibited different Nusselt numbers when compared to the isothermal experiment. To further study the difference, this project simplifies scale for the TLC experiments which will be run on a 2-inch panel-similar to Smith's setup but with the warm-band TLCs from Lawler's experiments.

Figure 1. Rotating Full Scale Serpentine Passage Test Section

One of the challenges associated with TLCs is the calibration procedure and sensitivity. Hay et al. show results using dimensionless equations to create calibration equations due to the calibration curve displaying shapes independent of active range in which TLCs display colors (Hay & Hollingsworth, 1996). Since cameras detect different hue values from different angles even if the color of the surface does not

change, it is essential to perform in-situ calibrations. Kakade et al. present effects of varying angle, light intensity and frequency on TLC calibrations. You et al. utilize a pixel-by pixel calibration where the TLC paint is heated in increments of 1°C and a camera records the image when thermal steady state is reached on the plate (You, Li, Wei, & Tao, 2017). This method enables the creation of hundreds of calibration equations (one for each pixel) and eliminates the effects of varying angle and light exposure. Previously at the GTL, Celestina et. al developed a benchtop facility that creates a linear temperature gradient on the TLC by running Syltherm XLT fluid at two different temperatures across the rear part of the channel (Celestina & Reagans, 2015). Full-scale experiments are reduced using the benchtop calibration. However, this project will use a novel transient calibration where a FLIR IR camera records the temperature across the TLC panel on the backside and a GoPro camera reads the hue values on the front side of the panel. For this method, conduction through the thickness of the TLC and black paint is negligible due to the minute thickness of the paint (less than 1 mm).

Once the hue data from the TLCs has been converted to surface temperature, Stasiek et al. propose using a one-dimensional conduction model to calculate the heat transfer for each pixel based on the initial fluid and wall temperature and the wall temperature profile in time (Stasiek & Kowalewski, 2002). as well as a formula using wall thickness, initial fluid and wall temperatures and the wall temperature profile. Kakade et al. uses Fourier's conduction equation for a semi-infinite solid in their application for narrow band TLCs on a rotating disc (Kakade, Lock, Wilson, Owen, & Mayhew, 2009). At the GTL, Lawler utilizes the DuHamel superposition method, an iterative solver that utilizes steps in wall temperature and fluid temperature to calculate heat transfer coefficient, to solve for heat transfer in a transient setting. This project will use the Cook-Felderman method originally derived for thin film heat flux gauges (Haldeman, 2006). The advantage of the new method is the decrease in computational time while maintaining accuracy, as will be presented in the methodology section. You et al. used an energy balance to calculate the local bulk fluid temperature by estimating heat losses and measuring the heat provided by the heater

for steady state TLC measurements. This project will continue with the assumption of a linear change in fluid temperature from inlet to outlet proposed and verified by Smith et al.

1.2 Research Purpose and Objectives

The main purpose of this research is to compare the single panel TLC results with the isothermal single panel experiments being conducted by Howard. In the past, it has been difficult to directly compare the two experimental techniques due to differing flow entry conditions. However, the inlet conditions should be the same for the two simple geometries investigated in this project since the inlet geometry is the same, inlet flow conditions and mass flow rates are identical. To compare the results, area averaging will be used for the TLCs to compare to the single point result available in the copper panel experiments.

Another purpose for this project is to verify any visual based post-processing methods that have been utilized in the full-scale test section. Verifications on these panels are significantly easier due to their compact size and having the ability to tinker with the test section and perform many small experiments. Verifying the different camera corrections applied to previous data is vital because the temperature, and thus the heat transfer, is derived directly from the camera feed.

Chapter 2: Methodology

Chapter 2 discusses the methodology followed to assess heat transfer in the panels. The calibration process and results for smooth and turbulated panels are discussed, the heat transfer algorithms are introduced, and the visual and data reduction procedure is outlined in this chapter.

2.1 Calibration Overview

Previously at the GTL, TLCs were calibrated using a steady state benchtop facility (Celestina and Reagans, 2015). A copper plate is painted with TLCs and Syltherm XLT heat transfer fluid is circulated through both ends of the plate: the fluid at one end is heated and at the other end is cooled. This action generates a temperature gradient across the plate, which is visible in the color of the TLC in Figure 2. The white dots at the left and right ends of the TLC band are resistance temperature detectors (RTDs) that record temperature at that point. Once the conduction between the hot and cold fluid paths reaches steady state, the temperature gradient between the two ends becomes linear. This means that a linear fit can be applied vertically across the plate to determine temperature values at different points along the TLC band. These in turn can be used to correlate the hue of the TLC to the temperature of the surface. This experiment is performed in a vacuum chamber to eliminate the influence of convection on the surface temperature of the plate.

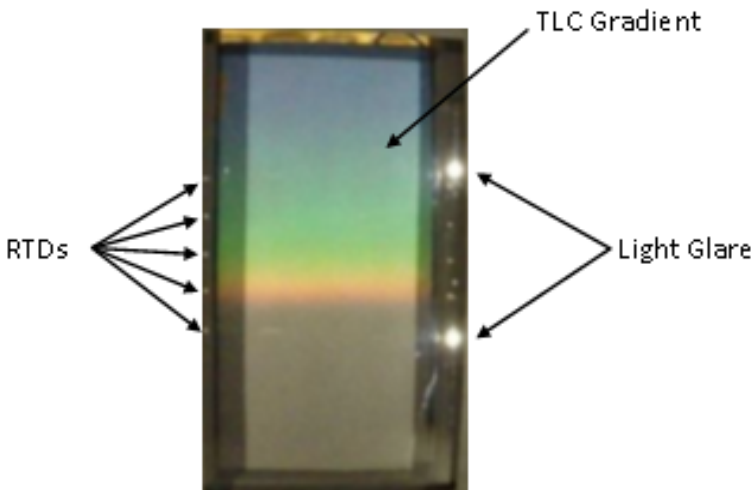

Figure 2. Steady State TLC Calibration Image

A transient calibration method will be employed for the current project to potentially enable a more precise fit and make it easier to replicate the positioning and lighting of the real experiment. A picture of the calibration setup is seen in Figure 3.

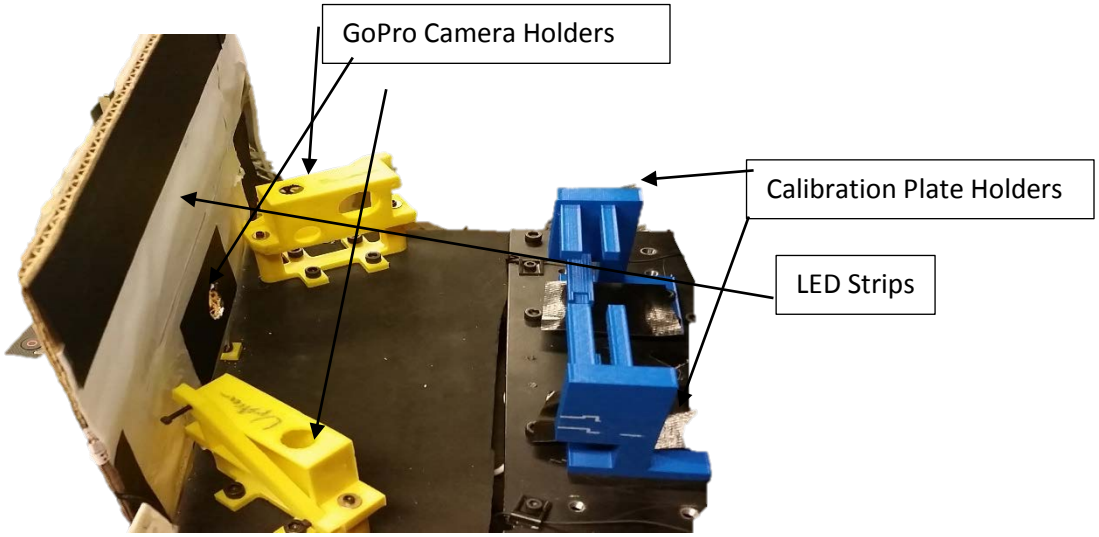

Figure 3. Transient TLC Calibration Setup

The lighting and camera mounts in this setup are mounted to a plywood sheet covered with black foam to ensure minimum reflectivity. In turn, this plywood is mounted to the black 6061 Aluminum

baseplate that anchors the test article to support and ensure that no movement takes place during the experiment and calibration runs. The vertical cardboard wall in Figure 3 houses the LED strips and is fixed into place by the three yellow camera holders (center camera holder is hidden behind black paper). To test light placement and setup, several videos are acquired which record the effect of changing the supply voltage for the LED strips as well as different diffuser setups. In the current setup, black construction paper and regular printer paper are used to diffuse light as much as possible. To keep the lighting scenario similar to the full-scale rotating test section, LED strips are positioned below and above the camera. Figure 4 shows the lighting setup and the placement of the printer and construction paper. With this setup, any potential movement of the cameras and lighting, which can adversely affect hue measurement between runs and calibrations, is minimized.

Figure 4. Transient Calibration Setup with LED Lights

The two blue holders seen in Figure 4 were designed such that the distance from the acrylic panel to the center of the camera will not change whether the holders were used during calibration or the full frame is used during a run. Additionally, a FLIR A655sc infrared camera is placed at the opposite side of the GoPro holders to detect the temperature. The camera is exposed to the backside of the acrylic panel

and records temperatures at 12 frames per second for a duration of 30 minutes. On the front side of the acrylic panel, a GoPro camera is mounted in the camera holder and captures video at 60 frames per second with a narrow field of view to record the changing hue in the panel. A SolidWorks sketchup of the model is shown in Figure 5; the LED strips are not included in the CAD drawing.

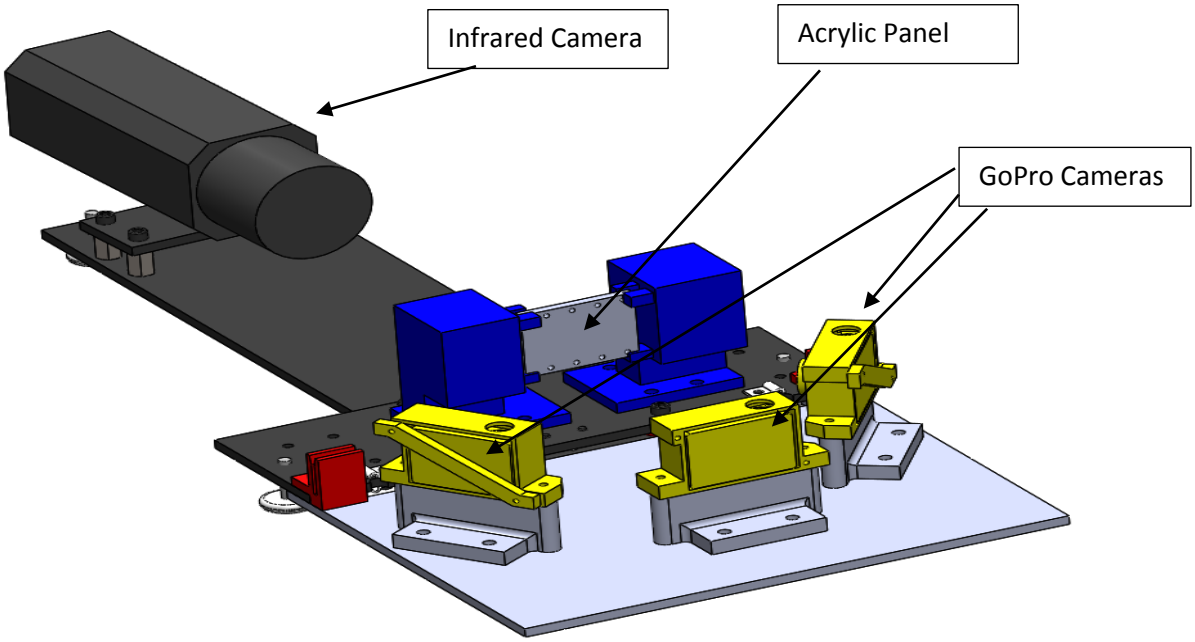

Figure 5. SolidWorks Model of Calibration Set-Up

The IR camera records are imported into MATLAB using FLIR ResearchIR software. Due to the data size constraint of MATLAB (maximum file size cannot exceed 2 GB), a frame anywhere from every 1.05 to 1.181 seconds is imported into MATLAB. A single frame from the IR camera can be seen in Figure 6. The synchronized frame from the GoPro video for the same calibration is seen in As predicted, the temperature at the ends of the passages is the lowest due to their contact with the PLA printed holders, whereas the middle of the passage is only exposed to free convection and lateral conduction and is therefore slower to cool. To accurately synchronize the IR camera feed with the GoPro feed, the lights are used as the starting point for the GoPro video. Similarly, the lights also act as the starting point on the IR camera. However, this is not possible to perform without manually examining the first few frames. After

examining the first few frames, it is possible to see the LED strips as dim dots in their respective positions as seen in Figure 8. After the first frame with LED strips is detected, the video is then synchronized and imported into MATLAB. After MATLAB loads the IR temperature data, a code is used to find how much time has elapsed between each imported frame. This matrix is then used to modify an existing fisheye correcting video editor code such that each time value calculated by the IR code is then used to skip to the appropriate frame in the GoPro video feed. Therefore, the video from the GoPro is not played in real time, instead the video is accelerated such that every frame corresponds to every imported frame from the IR. This process reduces the approximate duration of the GoPro video from 30 minutes in real time down to 25 seconds.

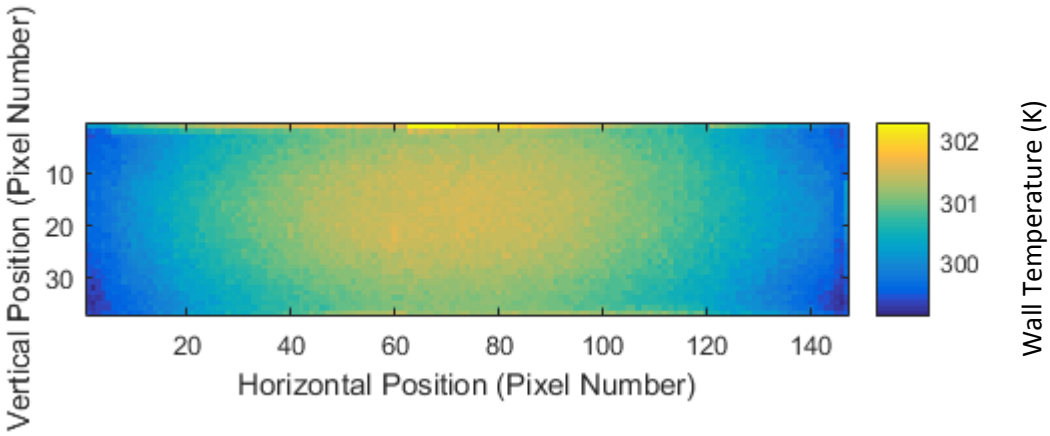

Figure 6. Infrared Camera Temperature Measurement Contour Plot

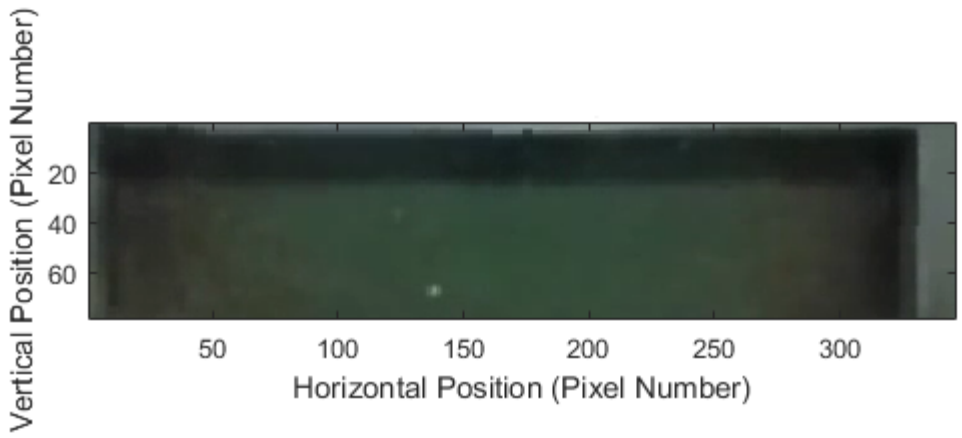

Figure 7. GoPro Video View of Smooth Panel

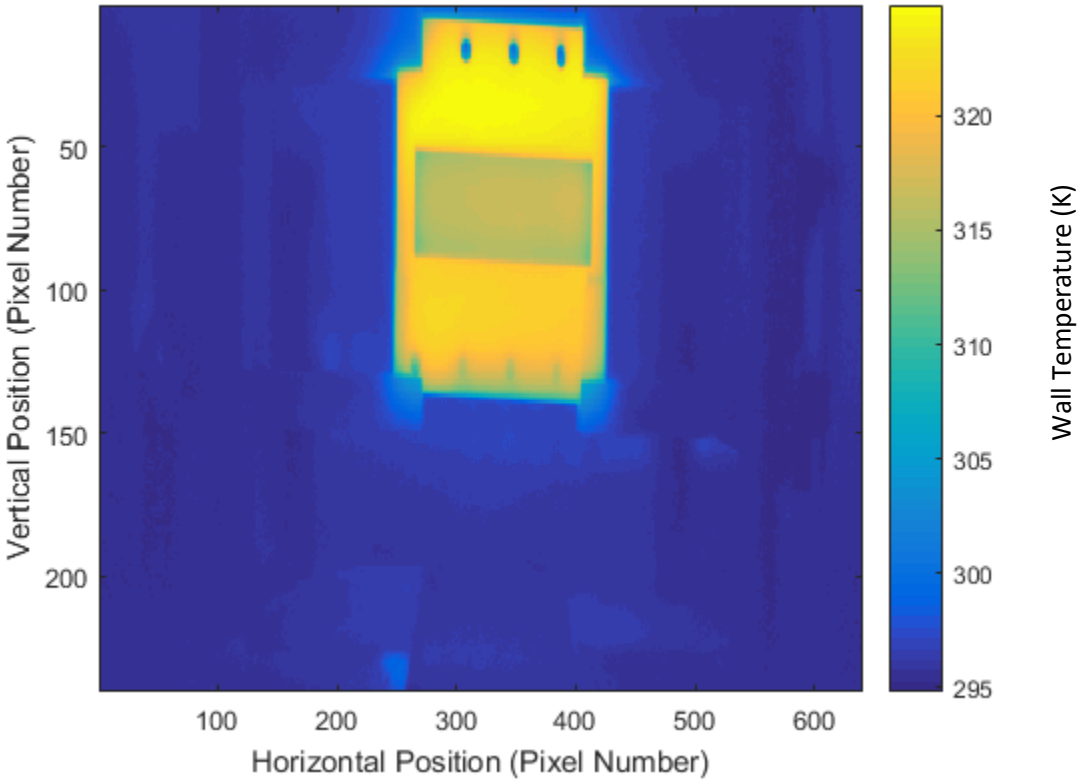

Figure 8. IR Camera Calibration Starting Frame

Initially, a pixel by pixel fit was attempted using the "2dinterp" function in MATLAB. However, this did not result in a successful calibration because the sizes of the IR matrix and the GoPro feed were not a multiple of each other as required by the function. Instead, an area averaging calibration method is used.

To calibrate the IR and GoPro feeds, both feeds are cut into 18 sectors and each sector is assigned an average Hue value (GoPro feed) and an average temperature value (IR feed). This process is then repeated for all frames in both feeds. This way each sector is given average hue and average temperature at each time step. MATLAB codes were created to split both feeds into sectors, and then the sectors are refined to exclude shadows. A 12-sector calibration is initially attempted but the fit is poor across the sectors due to excessive shadow regions in the sector. To counteract the shadow problem, an 18-sector calibration is introduced with the side sectors containing the shadows. The sectors are named from top left to bottom right. A map of the sectors can be seen in Figure 9.

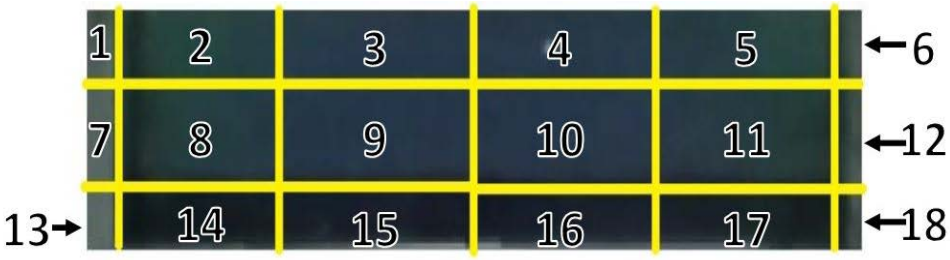

Figure 9. Area Averaging Sector Calibration Map for Smooth Panels

The process of calibration begins with heating up the acrylic panels in the toaster oven seen in Figure 10. A thermocouple is attached to the toaster oven to monitor the temperature so to not overheat the panel. A temperature of 140 °F with a tolerance of 5° is maintained in the heating process. After the panel reaches the upper limit of the activation range, it is removed and placed in the blue holders shown in Figure 3. While the panel is heating up, the GoPro and IR feeds are setup, and then recording starts roughly 10 seconds after the panel is placed in the holder. This 10 second delay is due to how much time is required to go from the calibration setup to the main computer to start the IR feed. The panel sits in the holder for approximately 30 minutes (the time required for the panel to reach ambient temperature) and then the IR camera and GoPro camera stop recording.

Figure 10. Toaster Oven with Thermocouple

2.2 Calibration Results

Once data acquisition is complete for the calibration, the IR data is imported into MATLAB and the GoPro feed is cropped and corrected in GoPro Studio and MATLAB. An issue with the IR camera is the duration of the calibration and how the IR camera auto-focuses on the image every few minutes. This action causes the IR feed to experience a sudden drop in temperature. To alleviate this, each sector temperature is manually increased by the drop in each spike during the calibration. This achieves a realistic temperature fit. A plot of the raw IR data and the manually fixed IR data from sector 10 and calibration 3 of the smooth panel can be seen in Figure 11. To correct the issue in further calibrations, the "AutoNUC" feature on the IR camera was turned off for long duration recording. This prevented the camera from correcting frame temperature values incrementally.

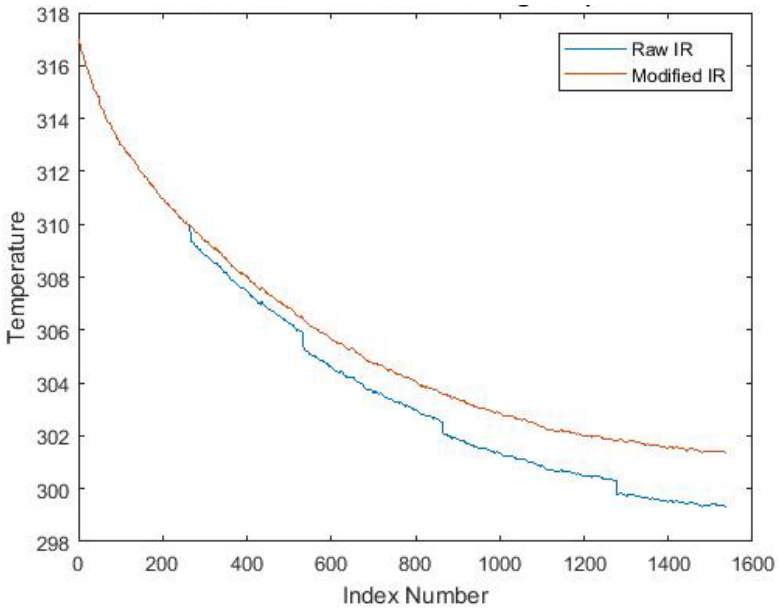

Figure 11. IR Raw Temperature and Modified Temperature Comparison

The average hue value of the same sector can be seen below in Figure 12. The hue fluctuation near the end of the calibration is due to the TLC passing through the lower range of the activation range. Hue is undefined for pure black, so as the image gets darker, the Hue can swing wildly for small changes in appearance.

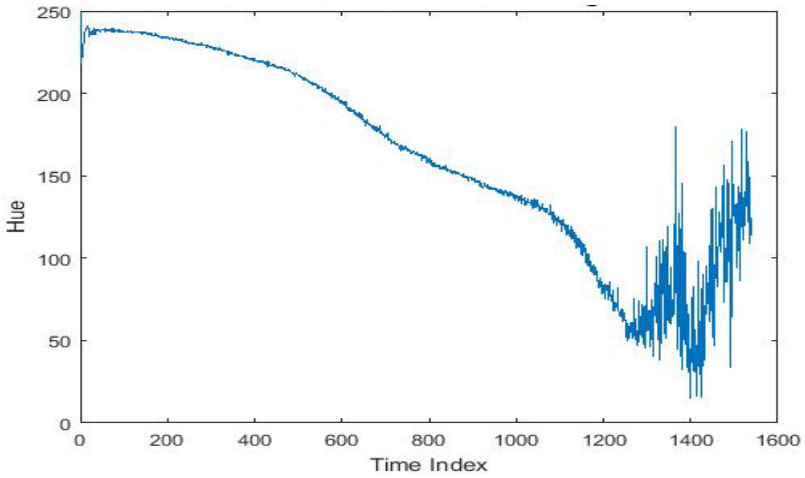

Figure 12. Average Hue for Smooth Panel Calibration 3 Sector 10

Each sector's hue and temperature are plotted against each other in order to create a fit for each sector. The results of sectors 1 through 6 of Calibration 3 are shown in Figure 13. Sectors 2 through 5 exhibit similar trends and values whereas the edge sectors are showing higher hue values at roughly the same temperatures. This is due to the acrylic included in the corner sectors. Similar results are shown in Figure 14 for sectors 7-12 and in Figure 15 for sectors 13-18. Figure 15 also displays the calibration range for the fits. A range of 302 K to 309 K is applied to every sector to create a fit. A MATLAB code will find indices that match the given input condition for the range and then create an appropriate matrix based on the indices.

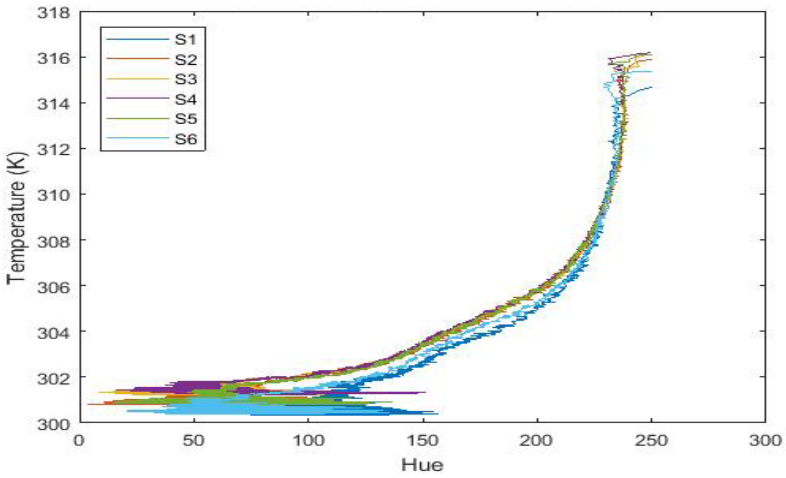

Figure 13. Smooth Panel Calibration 3 Sectors 1-6 Results

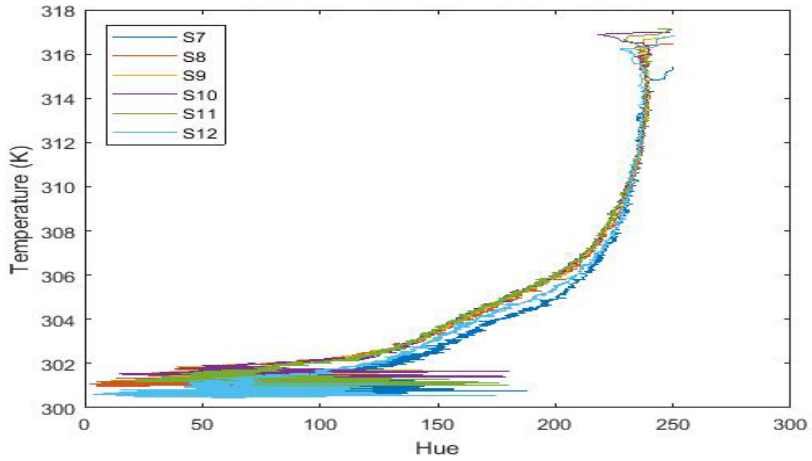

Figure 14. Smooth Panel Calibration 3 Sectors 7-12 Results

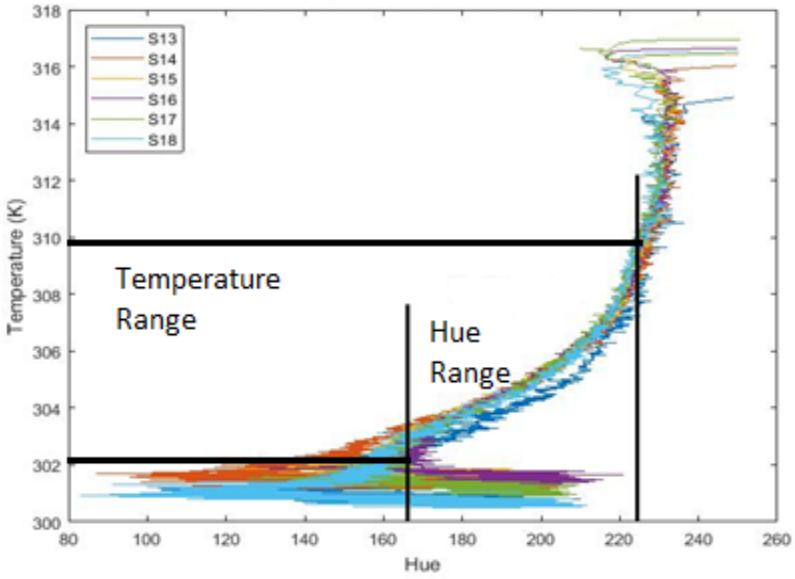

Figure 15. Smooth Panel Calibration 3 Results Sectors 13-18 Results

Fourier fits are used to quantify the relationship between hue and temperature. First to fourth order results from calibration 3 sector 10 are shown in Figure 16, and fifth to eight order results are shown in Figure 17. In order to maintain continuity with experiments completed by Lawler and calibration fits used by Celestina and Reagans, an 8th order Fourier fit will be used in heat transfer algorithms.

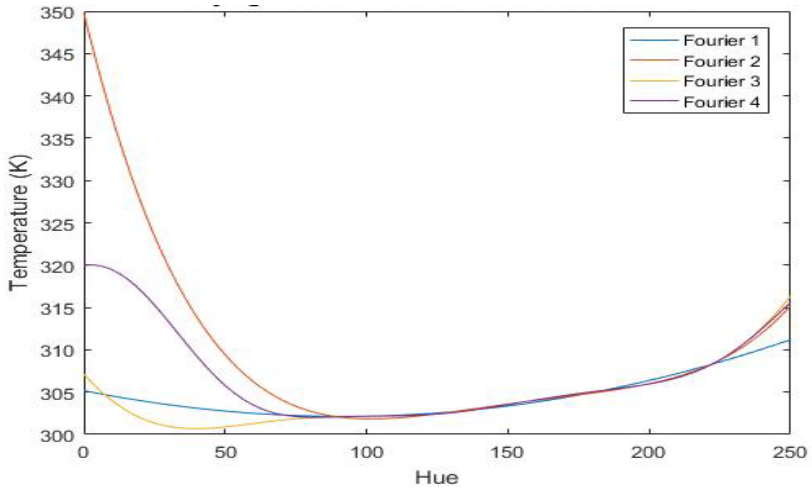

Figure 16. 1st-4th Order Fits for Calibration 3 Sector 10

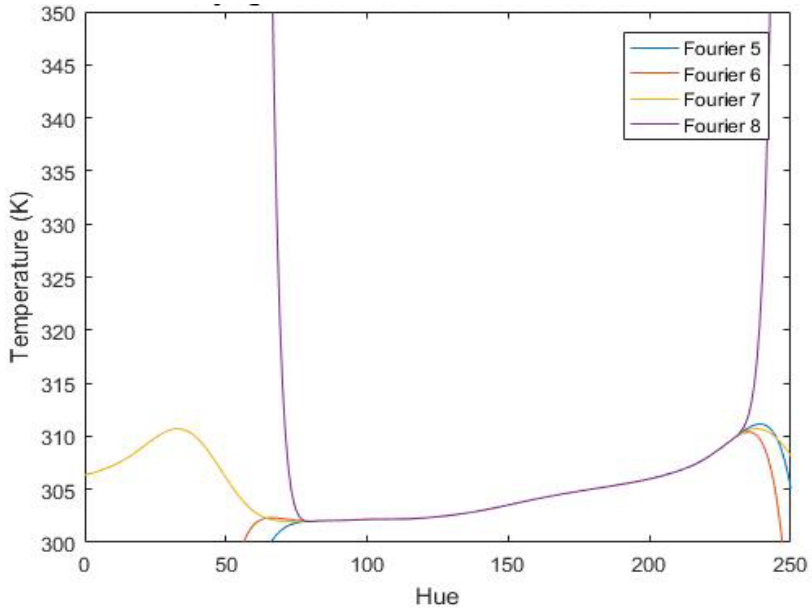

Figure 17. 5th-8th Order Fits for Calibration 3 Sector 10

For turbulated panel calibrations, a different sector map was used and is seen in Figure 18. The sectors were chosen to be restricted to smooth and turbulated sections due to any temperature gradients that could arise when cooling the panel. The same method of averaging hue and temperature was used as well as the 8th order fourier fit. The results from the turbulated panel calibrations are shown in Figure 19. There are 9 sectors included in the plot, corresponding to each sector in Figure 18.

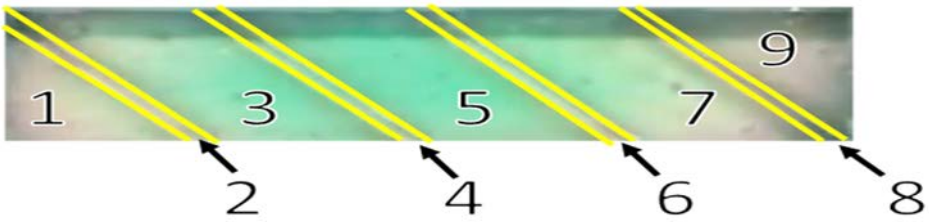

Figure 18. Turbulated Panel Calibration Sector Map

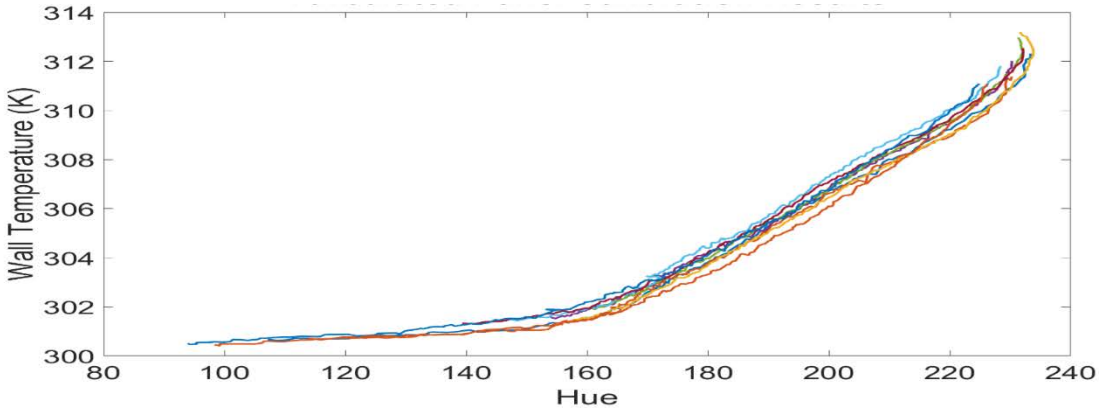

Figure 19. Turbulated Panel Calibration Results

2.3 Heat Transfer Algorithms

To calculate the heat transfer, the Cook-Felderman algorithm (Haldeman, 2006) will be used. Lawler used DuHamel superposition that relied on fluid temperature as well as step sizes to iteratively calculate the heat transfer. At its root, the DuHamel method is a solution of the equation for semi-infinite conduction with a known surface heat transfer coefficient shown in Equation 1**.** The equation is solved implicitly using the golden bisection rule where a heat transfer coefficient value (h) is guessed and then the right-hand side is evaluated to give a difference in the wall temperature at that time step with the wall temperature at the beginning. If this solved value is correct, then the equation is deemed solved, otherwise the program keeps iterating until the evaluated right-hand side of the equation matches the actual temperature difference measured by the TLCs on the left-hand side.

Equation 1. DuHamel Method

$$T_{wall} - T_0 = \sum_{i=1}^{n} \{1 - \exp\left(\frac{h^2 \alpha (t - t_i)}{k^2}\right) erfc\left(\frac{h\sqrt{\alpha (t - t_i)}}{k}\right)\} (T_{Fluid_i} - T_{Fluid_{i-1}})$$

The Cook-Felderman algorithm is shown below in Equation 2 and is an explicit solver that determines heat flux based on the semi-infinite conduction model for a constant surface temperature. It relies only on the time rate of change of wall temperature to solve for heat flux and therefore does not have to iterate for each time step, offering large computational savings. This algorithm was originally developed for thin film heat flux gauges and is being used for the first time in this application.

Equation 2. Cook Felderman Equation

$$q'(t_n)_{uncor} = 2\sqrt{\frac{|\rho c k|_{ref}}{\pi}} \sum_{i=1}^{n} \frac{T(t_i) - T(t_{i-1})}{(t_n - t_i)^{\frac{1}{2}} + (t_n - t_{i-1})^{\frac{1}{2}}}$$

This algorithm was verified using two different methods: the first method was to check the algorithm with the constant surface heat flux semi-infinite solid formula and the other method was to check the algorithm with the DuHamel results from one of Lawler's datasets. The constant surface heat-flux formula used for the first step of algorithm verification is shown in Equation 3. The x value is set to 0 to evaluate the heat flux at the surface only and the q''_0 value is set to 500 to verify that Cook-Felderman returns 500. Using these values, a fake temperature profile is created and then put into Cook-Felderman to evaluate the heat flux. The results of the verification method are shown in Figure 20. Cook-Felderman returned values of 500 with a tolerance of 0.25 for the majority of the calculation. There are inconsistencies with the first three time steps but they are deemed to be negligible because the averaging window for this experiment does not cover the initial range.

Equation 3. Constant Surface Heat Flux Semi-Infinite Solid Formula

$$T(x,t) - T_i = \frac{2q_0''\left(\frac{\alpha t}{\pi}\right)^{\frac{1}{2}}}{k}\exp\left(-\frac{x^2}{4\alpha t}\right) - \frac{q_0'' x}{k} erfc\left(\frac{x}{2\sqrt{\alpha t}}\right)$$

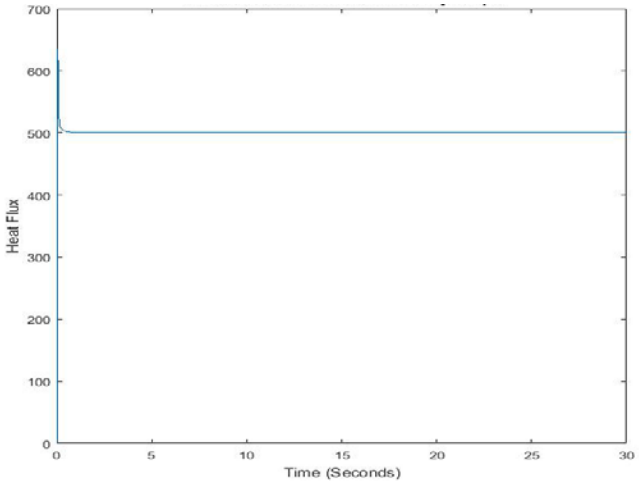

Figure 20. Verification of Cook-Felderman Algorithm with Semi-Infinite Solid Formula

The results of the DuHamel algorithm values compared to the Nusselt number values from Cook-Felderman are shown in Figure 21**.** The main advantage of the Cook-Felderman method is the speed. Computational time can be reduced by almost 90% while solving for every pixel unlike DuHamel.

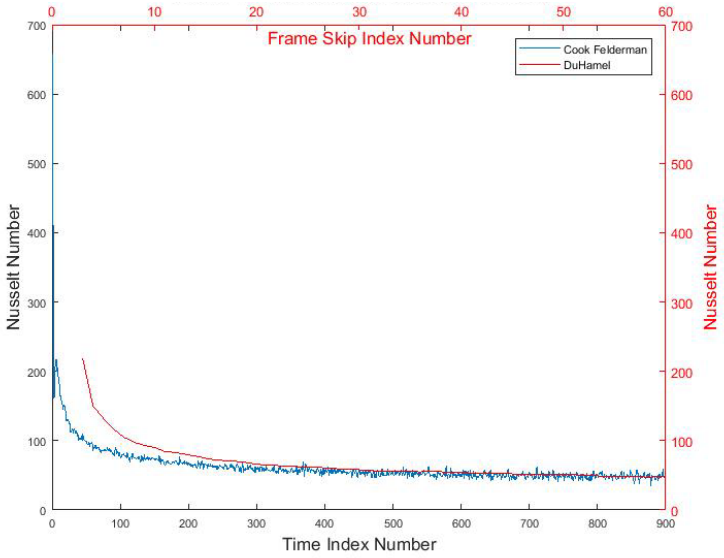

Figure 21. DuHamel and Cook-Felderman Comparison for Panels

2.4 Data Reduction Procedure Overview

The method to reduce a run follows the model shown in Figure 22. First, the GoPro video is corrected using a newly found "lensdistort" function. The function had been used first at the GTL by Sperling. The previous method was to use a toolbox by David Scaramuzza, but the lensdistort method was deemed better due to a reduction in processing time and its ability to customize the intensity of fisheye correction. The second step is to generate a wall temperature matrix from the corrected GoPro videos. The appropriate calibration equation for each pixel is used to calculate the temperature based on the hue. After the wall temperature history is created, the fluid temperature matrix is created by assuming a linear fit between the two thermocouples (Smith et al., 2013). This fit was used by Lawler and was proven to appropriately capture the data. The thermocouples are located approximately an inch into the inlet so there is an inch between the upstream measurement location and the start of the TLC panel, and an inch between the end of the panel and the exit temperature measurement. However, for this experiment, it will be assumed that the downstream thermocouple matches the fluid temperature at the end of the

panel, and the upstream thermocouple matches the beginning of the panel. Due to the short length of the inlet exit and outlet entrance and their distance between the thermocouples, the assumption seems reasonable. After the fluid temperature matrix is created, the wall temperature matrix is written in delimited format and sent to FORTRAN's Cook-Felderman code to calculate heat transfer. After Cook-Felderman is complete, the heat flux matrix is read back into MATLAB and then, if applicable, turbulators are masked out using shadow detection results or manual picking of points. The final step is to reduce the heat flux data, along with masking and fluid temperature data to Nusselt numbers and then finding a good time averaging window.

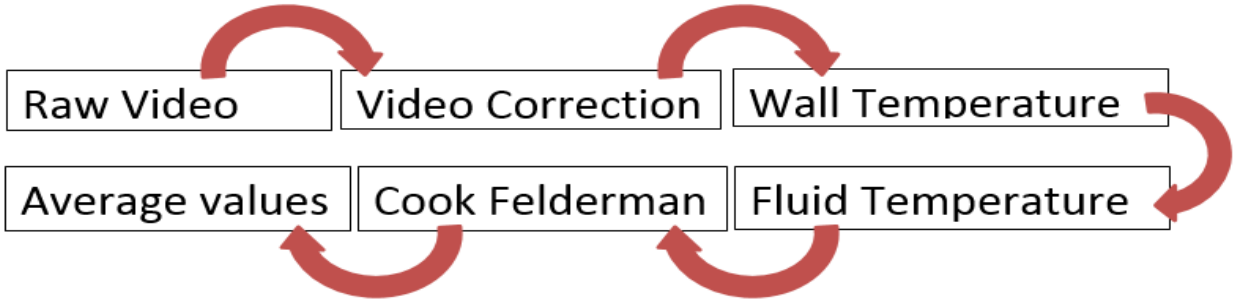

Figure 22. Run Reduction Flowchart

2.5 Visual Corrections

As mentioned earlier, the main disadvantage of the TLC is its sensitivity to camera position changes, lighting variation, and other external differences such as ambient light leaking into the test section. Over the past 2 years, work has been completed in correcting for camera effects. Currently, a code is being used which calls a lensdistort function which corrects the frame using the center point of the image and a distortion coefficient. A previous study was done on the full-scale test section, and a distortion coefficient of -0.32 was found to be the best. For all the single panel runs, a value of -0.32 will be used. In addition to fisheye corrections, throughout the full-scale test section, the video would often come in curving upwards after the fisheye correction. This effect, herein referred to as the "banana curve", was fixed by creating a program which would create two horizontal lines of reference, and then the script

will manually manipulate the matrix of each frame to fix the image in between the two horizontal reference lines to make a straight image. Due to the small length of the panel in the current experiments, the banana curve was not as noticeable therefore that function will not be used in the video correction part of the post-processing.

2.6 Experimental Setup

The experimental setup is shown in Figure 23. A choke is setup upstream of the test section with a maximum mass flow rate of .01 kg/s. Downstream of the test section is a vacuum chamber. Downstream of the choke and upstream of the inlet, there is a heater which is set to heat the air to 55 °C. A high-speed data acquisition system (DAS) will be utilized to capture data at 60 Hz for 40 seconds. When the experiment is ready to run, the DAS is triggered, the lights are turned on, and then the valve is opened to allow air through the test section. Since the lights are the trigger for the camera, there should be an indicator in the DAS for when the lights are turned on. To synchronize the DAS measurements with the camera recordings, the signal created by turning on the lights is fed into the DAS through a voltage-divider circuit. This circuit is created by a 10K Ω resistor and a 4.3V Zener diode in series with each other and in parallel with the LED strips. A picture of the circuit can be seen in Figure 24. When the voltage reading on the DAS is approximately 0 Volts, that means the lights are turned off and the airflow is bypassing the test section. When the voltage is approximately 4.3 volts, that means the lights have been turned on and the airflow is flowing through the test section. The timing for the voltage signal will then give the appropriate starting spot for the valves.

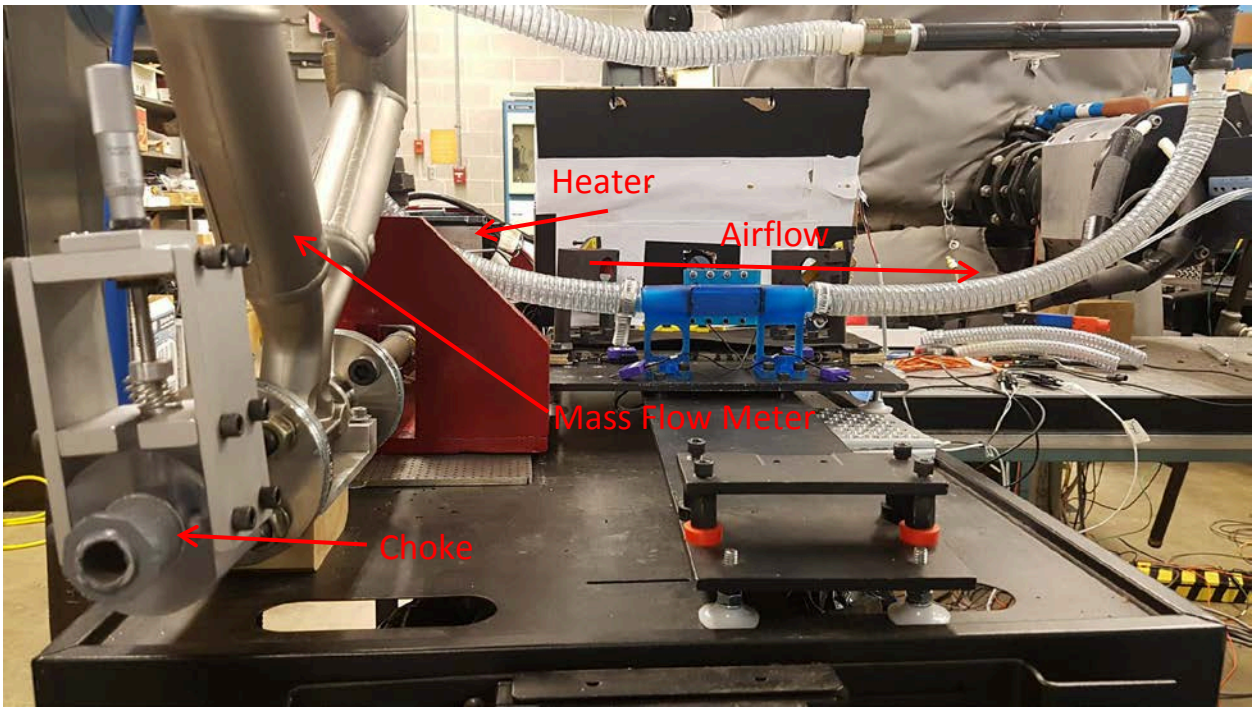

Figure 23. Picture of Experimental Setup

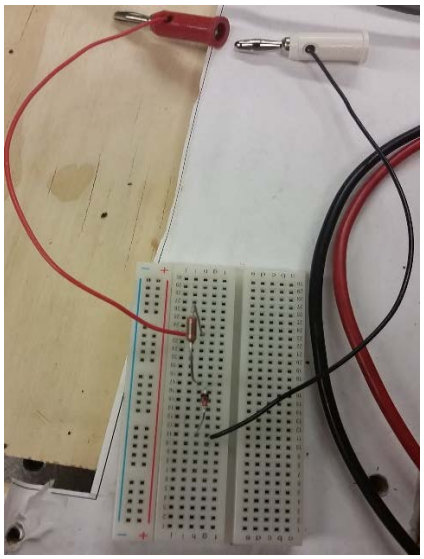

Figure 24. Circuit for DAS Voltage Signal

As mentioned before, this project will focus only on a 2-inch panel of a TLC painted acrylic surface. The smooth panel is shown in . The acrylic panel is painted with a warm band of TLCs that are active anywhere from 25° to 30°C with a range of 5°C. On the TLC paint, a 1mm thick layer of black paint is

applied to indicate when the TLC is inactive. The TLCs become clear above or below the activation range and allow the black paint to show through.

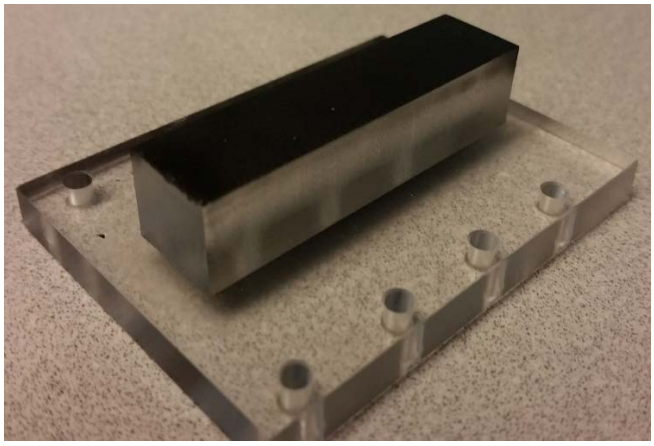

Figure 25. Smooth Panel TLC Single Panel

The inlets are shown in and were printed and utilized by Christensen. The inlets have thermocouples wired and feed voltage data into the DAS panel. The equation to convert thermocouple voltage into temperature is displayed in . Prior to using the equation, thermocouple voltage must be divided by 500 to account for gain.

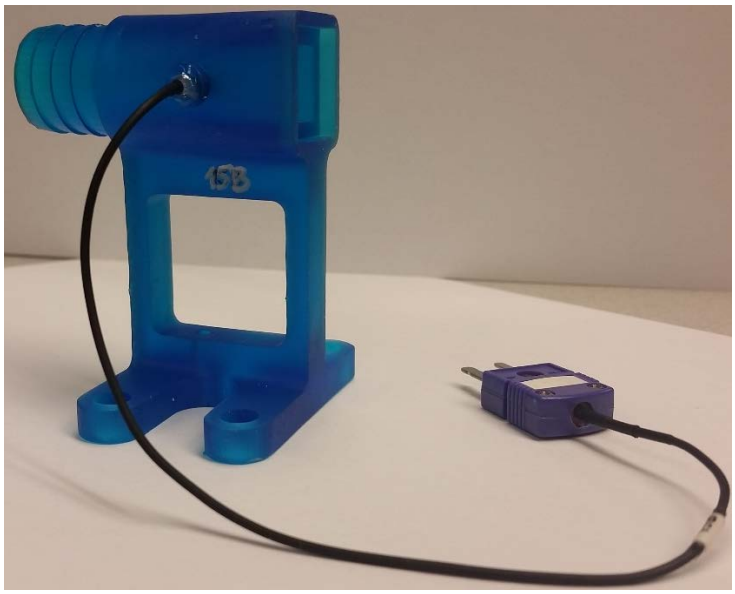

Figure 26. Test Section Inlet with Air Temperature Thermocouple Probe

$$Fluid\ Temperature = 273.15 + 17251.2v - 262553v^2 + 7836350v^3 - 99405296v^4\ [K]$$

Equation 4. Thermocouple Voltage to Temperature Equation

To hold the smooth panel in place between the inlets, a holder is designed and 3D printed using Formlab's tough SLA Resin. The 3D part is seen in . The attachment of the acrylic panel, holder and are seen in . Notice the black color visible through the panel window; this is due to the room temperature being below the activation range of the TLC, approximately 28°C. The O-ring around the panel is used to minimize leakage.

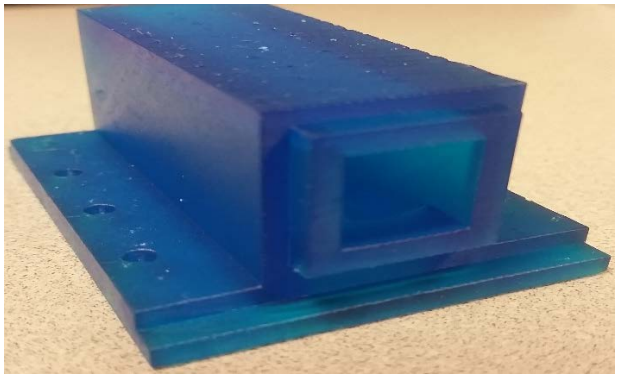

Figure 27. Smooth Panel Holder.

Figure 28. Acrylic Panel Assembly

Each run is performed using the routine shown in . Prior to every run, a black blanket is placed over the test section to minimize effects of ambient lighting. The same black blanket is used in the calibrations to maintain lighting consistency. Refer to for a visual of the setup for the blanket; a small hole is kept for the mass flow meter.

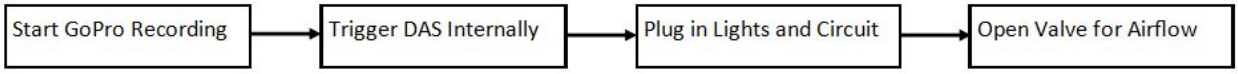

Figure 29. Experiment Routine

Figure 30. Black Blanket Setup

The power supply is run at 0.81 Amps approximately for every run to minimize lighting variation. The amperage varies anywhere from 0.80 to 0.82 Amps between runs. As mentioned before, the calibrations are run at the same current level.

For smooth panels, only the main camera is used since side data is not necessary. The panels are run at Reynolds number of 25000 and 50000. The Reynolds number is achieved by adjusting the choke position. For smooth panels, 6 runs are performed: 3 runs at 50000 and 3 runs at 25000. The same run conditions are repeated for the turbulated panel but with side cameras. The DAS captured thermocouple, mass flow, and voltage output from circuit at a frequency of 60 Hz for 40 seconds.

Chapter 3: Results

This chapter details the results in the smooth and turbulated panel results. Results detailed in this section are compared to the isothermal single panel experiment.

3.1 Results

A run matrix of the experiments conducted is shown in Figure 31. Data from Reynolds 35000 is not presented in this thesis due to incomplete processing. To initiate the trigger signal in the DAS, the circuit shown earlier is used. A plot of the DAS reading from the thermocouples and the circuit is shown in Figure 32. At approximately 4 seconds, the lights are triggered by connecting the banana pin connectors to the power supply, and the valve is opened at approximately 5.5 seconds. For purposes of post processing, the thermocouple data will start at the point where the voltage first spikes up. This ensures that the DAS is synchronized with the GoPro video.

Run #	Ambient Temp (F)	Heater Temp (Deg C)	Choke (in)	Reynolds Number	Smooth or Turbulated	Date and Time
15	75	55	0.149	25000	Smooth	3-2-18/10:20 AM
16	73	55	0.149	25000	Smooth	3-2-18/11:18 AM
17	73	55	0.149	25000	Smooth	3-2-2018/12:20 PM
18	75	55	0.234	50000	Smooth	3-2-2018/1:20 PM
19	75	55	0.234	50000	Smooth	3-2-2018/2:20 PM
20	75	55	0.234	50000	Smooth	3-2-2018/3:26 PM
21	75	55	0.183	35000	Smooth	3-3-18/10:30 AM
22	75	55	0.183	35000	Smooth	3-3-18/12:20 PM
23	75	55	0.183	35000	Smooth	3-14-18/12:40 PM
24	77	55	0.149	25000	Turbulated	3-27-18/5:45 PM
25	77	55	0.149	25000	Turbulated	3-28-18/10:00 AM
26	77	55	0.149	25000	Turbulated	3-28-18/11:10 AM
27	77	55	0.234	50000	Turbulated	3-28-18/1:20 PM
28	77	55	0.234	50000	Turbulated	3-30-18/10:34 AM
29	77	55	0.234	50000	Turbulated	3-30-18/12:25 PM
30	77	55	0.183	35000	Turbulated	3-30-18/2:01 PM
31	77	55	0.183	35000	Turbulated	3-30-18/3:31 PM
32	77	55	0.183	35000	Turbulated	3-30-18/4:56 PM

Figure 31. Run Matrix

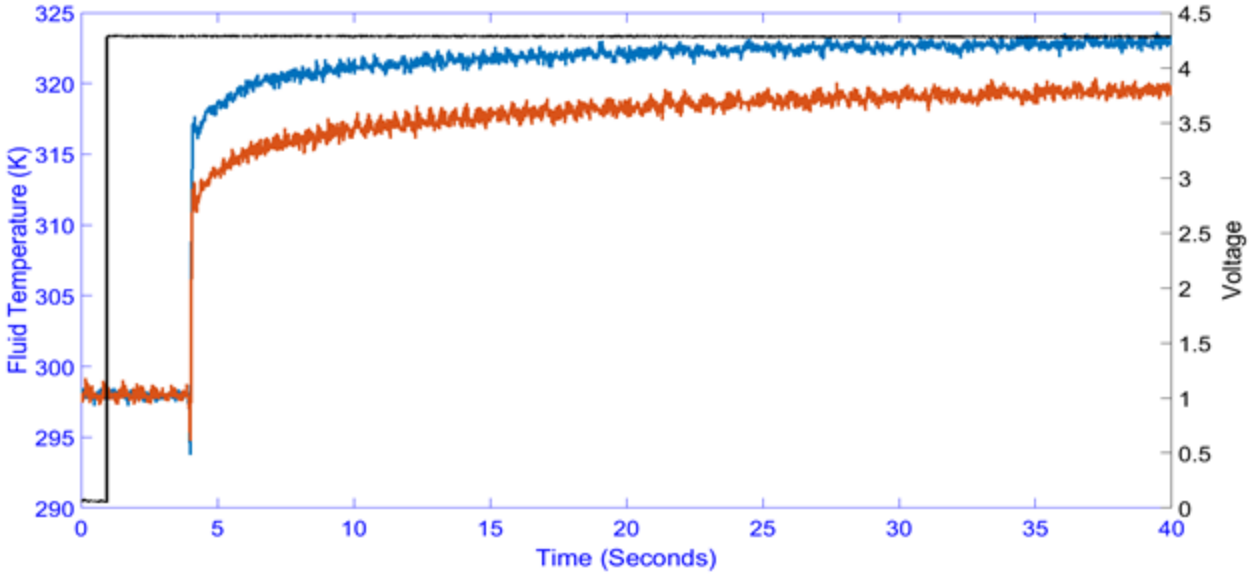

Figure 32. Timing Sequence showing Voltage and Thermocouple Data for Reynolds 50000 Turbulated Panel Run

In order to reduce the noise seen in the fluid temperature data in Figure 32, it is helpful to smooth the thermocouple signals in time using the MATLAB "smooth" function. Previous testing showed that the best results are obtained using the "loess" smoothing method with a time window span of 0.2. To smooth the fluid temperature data appropriately, the thermocouple output is broken into 3 sections: initial readings, valve opening spike, and post spike. Each regime is identified by a code that sets conditions by calculating finite differences, which can be specified by the user. Figure 33 shows the result of smoothing fluid temperature using the three different sections.

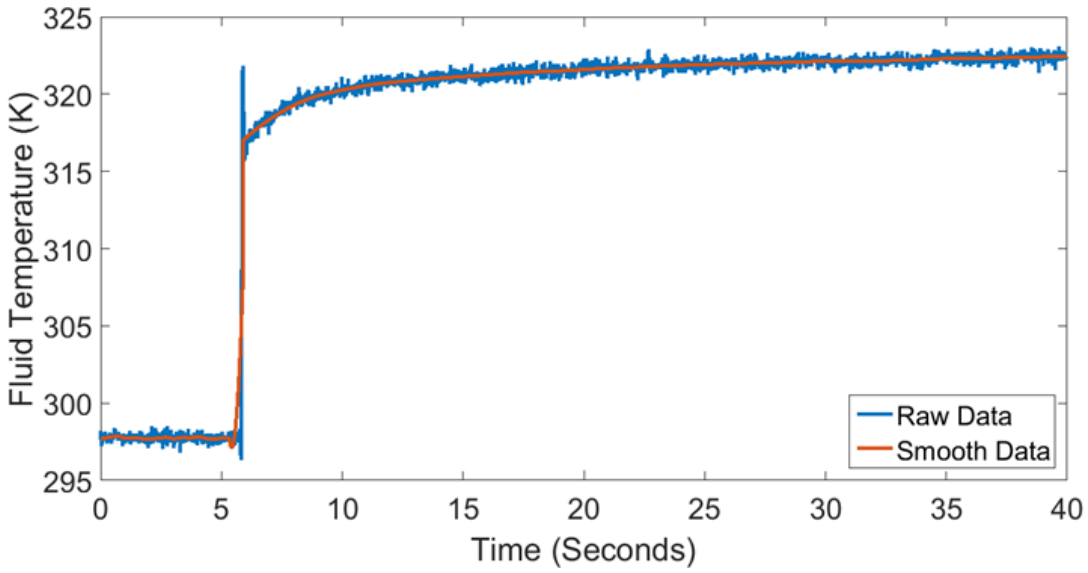

Figure 33. Fluid Temperature Smoothing Comparison for Reynolds 25000 Smooth Panel

After the thermocouple data is smoothed, a linear fit is applied for fluid temperature across the passage so that a local fluid temperature value can be determined for each pixel at each instant in time. The air is assumed to be at a constant temperature across the height of the passage and only change with the distance through the passage. Figure 34 shows the fluid temperature distribution across the panel for a Reynolds Number of 25,000. The fluid temperature decreases as it moves through the test section because heat is being transferred to the wall.

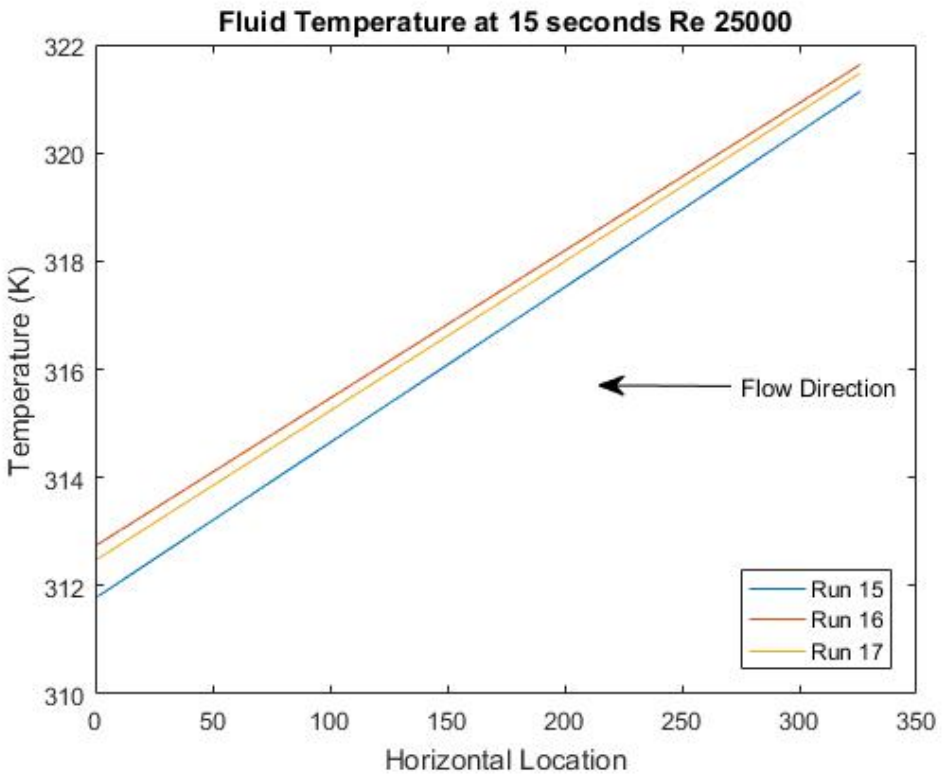

Figure 34. Fluid Temperature Distribution for Re 25000

A similar smoothing method is used for the wall temperature. The wall temperature measurements from the GoPro stair step through time due to the RGB response of the GoPro camera not being as precise. In other words, different RGB values will be detected in the camera but the same hue will exported by MATLAB. To fix this problem, wall temperature is smoothed through time for every pixel. The specifications used for smoothing the temperature are the same as fluid temperature but there are no conditions to separate the regime. A plot of wall temperature smoothing is seen in Figure 35.

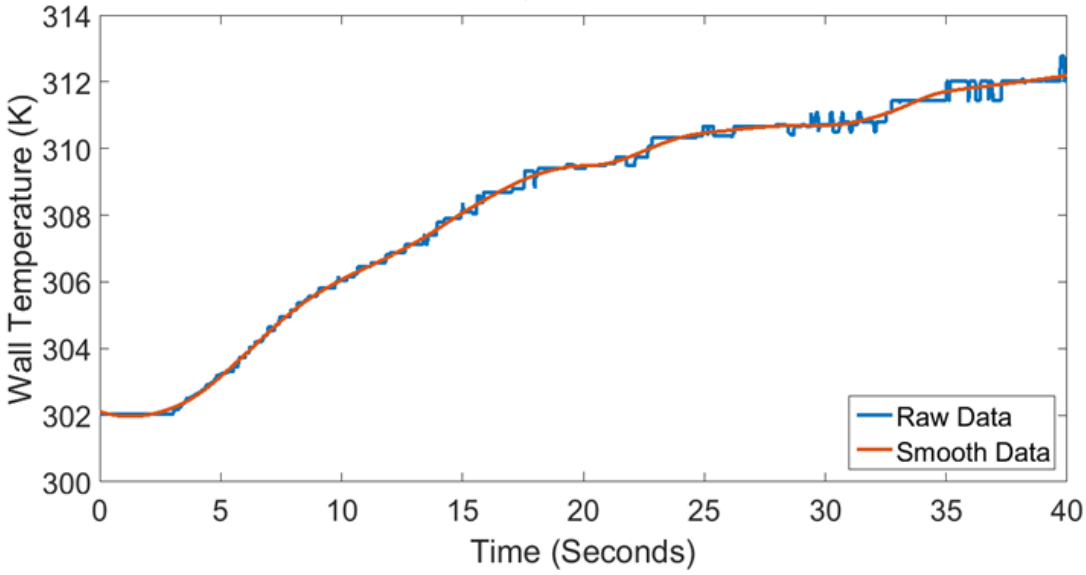

Figure 35. Raw vs Smooth Wall Temperature Data for Reynolds 25000 Smooth Panel

The mass-flow meter reading is converted from voltage to mass flow (kg/s) using Equation 5 and the Reynolds number is calculated using Equation 6. Refer to Figure 36 for mass flow rates for Runs 15-17 (Reynolds of 25000). There is some fluctuation seen in the plot however all 3 runs are giving mean mass flow rates ranging from .0046 to .0047 kg/s.

Equation 5. Mass Flow Conversion Equation

$$Mass\ Flow\ Rate = 5\left(\frac{V}{183.716} - .004\right)\left[\frac{kg}{s}\right]$$

Equation 6. Reynolds Number Equation

$$Re = \frac{4m}{\pi D \mu}$$

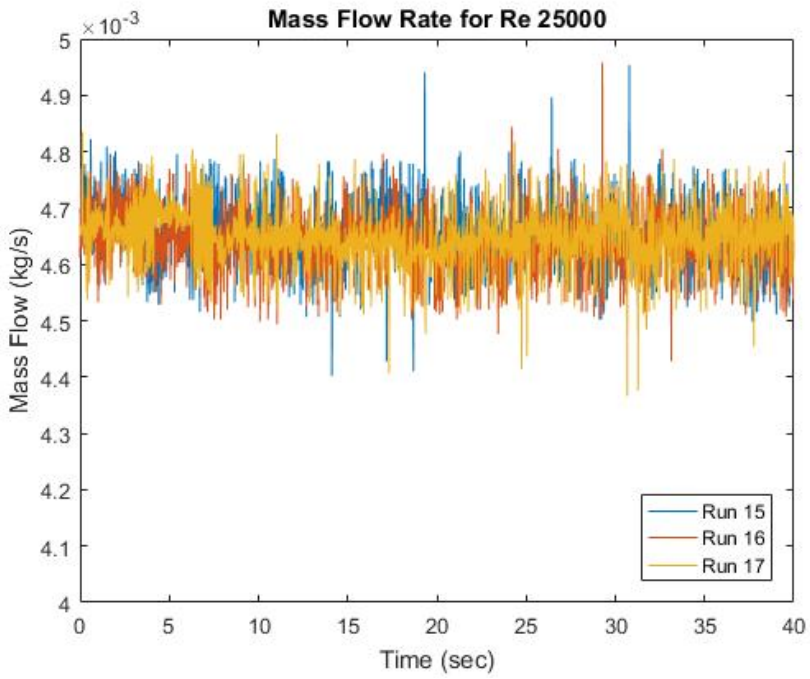

Figure 36. Mass Flow Rate for Re 25000

A plot of the Nusselt number across mid-span of the panel can be seen in Figure 37. Run 18 has a Reynolds number of 50000 and Run 17 has a Reynolds number of 25000. As expected, the Nusselt number for Run 18 is higher due to more mass flow through the channel. The spikes at either end are not understood completely yet. However, the fact that the spikes on the downstream side of the panel (left hand side of the graph) happen in relatively the same spot gives way to inference that the glare or presence of acrylic must affect the Nusselt number at the edges. To confirm this guess, the wall temperature distribution across the same mid span is plotted in Figure 38. As can be observed, the wall temperature is significantly higher for Run 18 than Run 17 due to an increase in mass flow leading to quicker rate of change of temperature. At both ends of the panel, it can be seen that the wall temperature drops the middle passage section. This confirms that the Nusselt number plot in Figure 37 has the sudden drops due to glares, shadows, and acrylic pieces present at the corners of the videos. One solution around this is to create a mask that will take out all Nusselt number values for the shadow region.

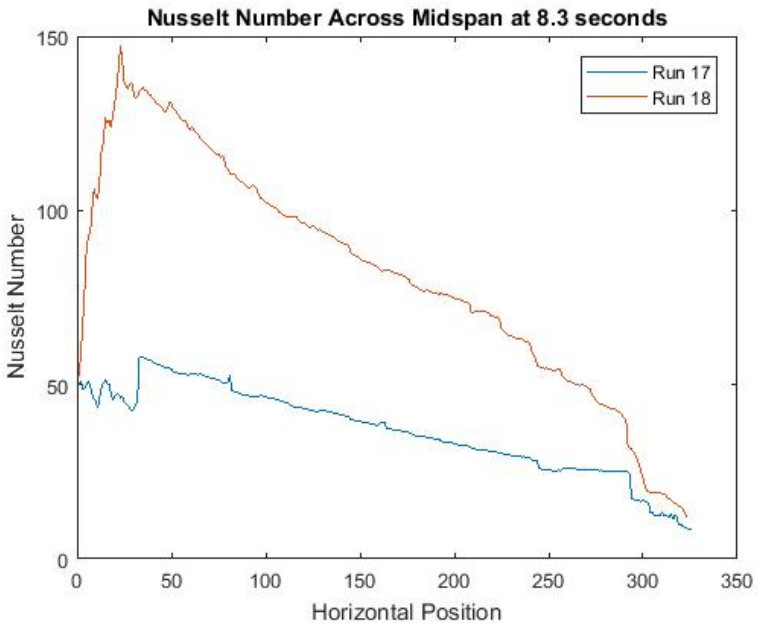

Figure 37. Mid-Span Smooth Panel Nusselt Number Comparison

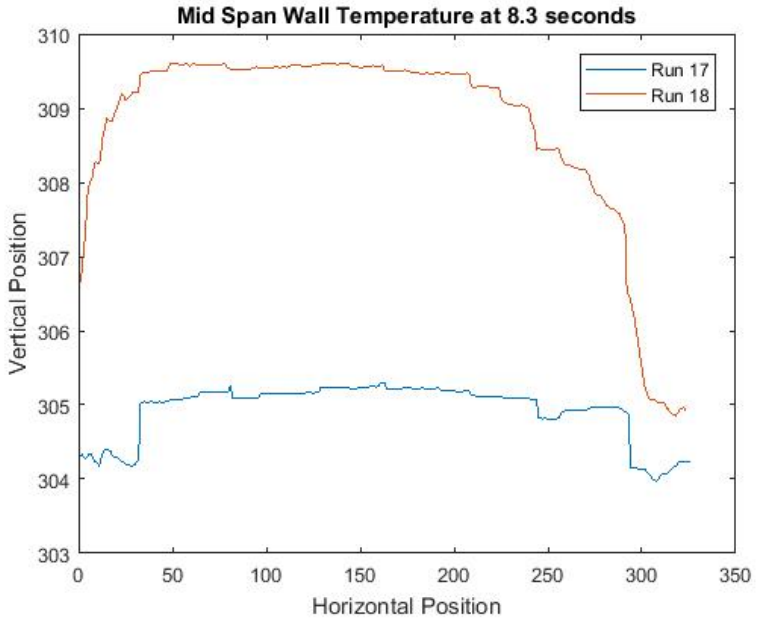

Figure 38. Wall Temperature Mid-Span Comparison

Since the temperature starts in the inactive range of the hue map, an initial analysis is applied to possible fits in the TLC. The three test conditions are called “pre-spike”, “linear fit”, and “post-spike”. These represent the three possible scenarios for the temperature to increase as the valve is initially opened. The three possible fits are shown in Figure 39. These three fits are input into the Cook-Felderman

algorithm and Nusselt number is calculated using the same fluid temperature values. The Nusselt number is shown to vary between 15.15 and 15.25 for all three fits so it is deemed that treatment of the uncertainty region at the beginning of the experiment has no effect on the Nusselt number averages.

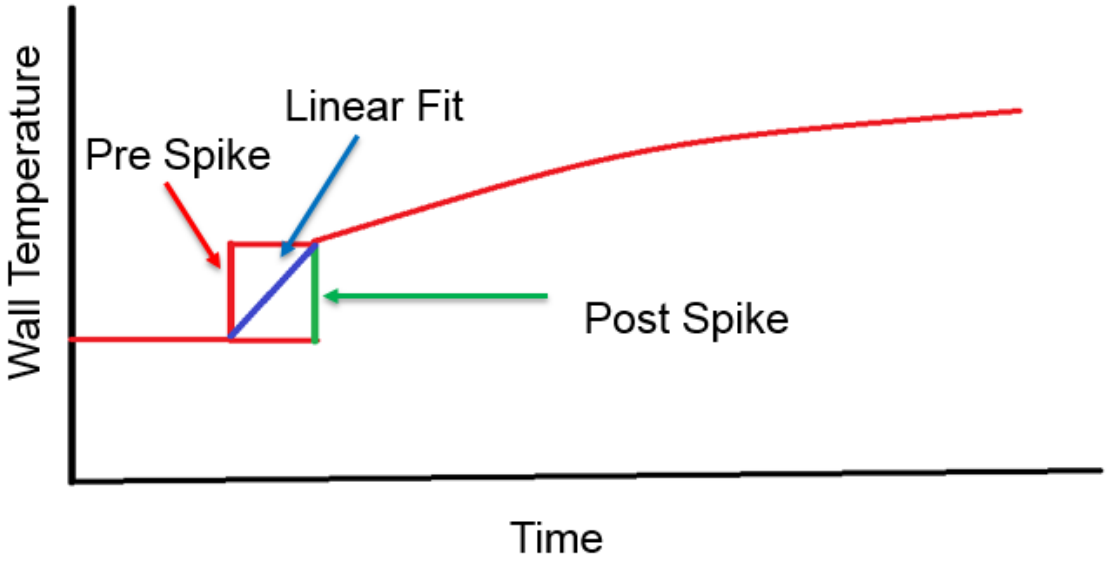

Figure 39. Initial Analysis for Wall Temperature using Three Possible Temperature Fits

The following series of plots show the distribution of Nusselt numbers across mid-span, 2/3rds span after different timesteps in the run. The Reynolds number for the specific line is shown in the legend and the parenthesis after indicate the type of panel (S for smooth and T for turbulated), and the numbers after the type indicate the run number.

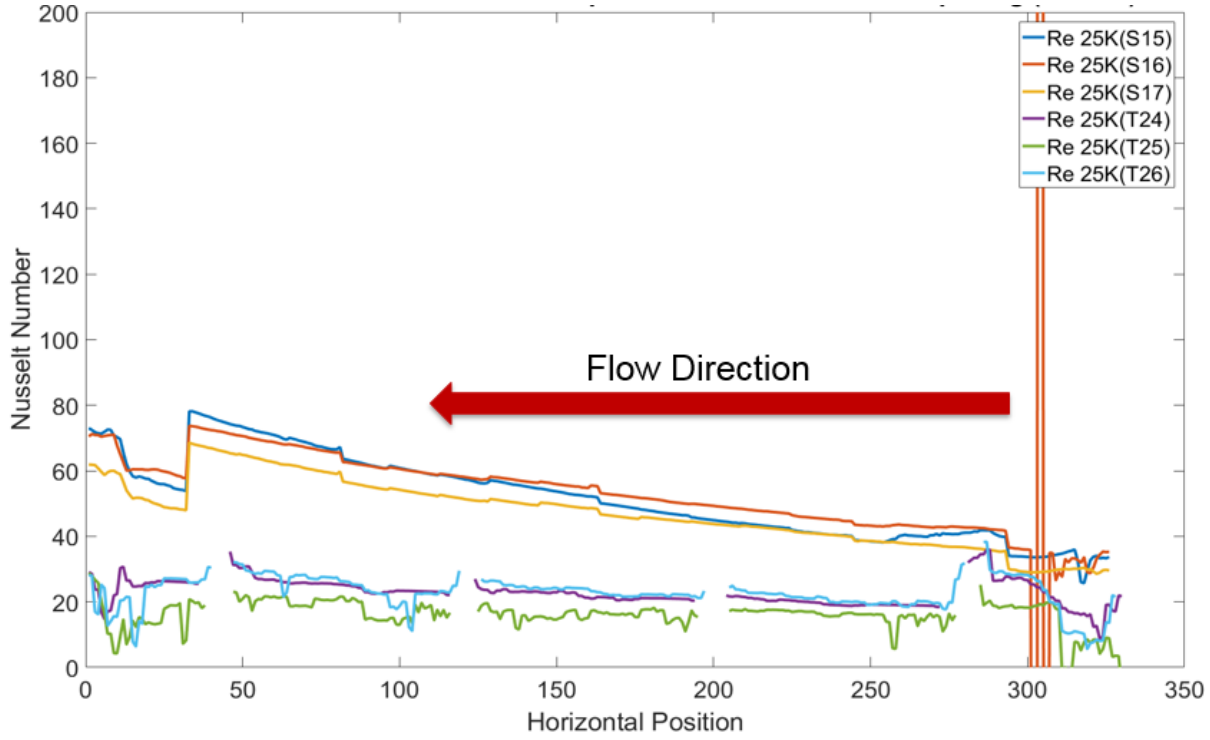

Figure 40. Turbulators vs Smooth Nusselt Number across Mid-Span 2 Seconds after Valve Opening at 25000 Reynolds Number

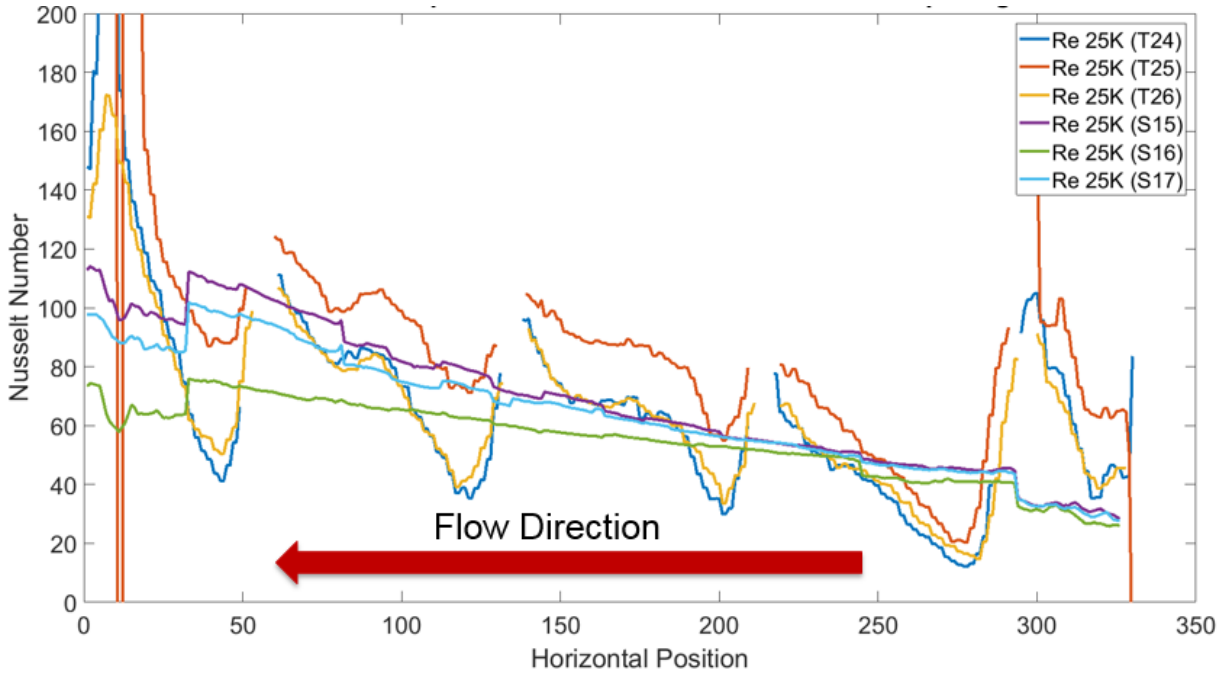

Figure 41. Turbulator vs Smooth Nusselt Number 2/3 Span-Wise Distribution 7 Seconds after Valve Opening at 25000 Reynolds Number

Figure 40 and Figure 41 show the effect of vortices induced by the turbulators and their respective locations with regards to Nusselt number. As can be seen, the 2/3rds span experiences higher Nusselt number downstream of the turbulator than the smooth panel does. This is indicating that the vortices from the turbulator are having their strongest effect near the bottom of the passage. In addition, there is a small region where the Nusselt number drops immediately after the turbulator. This is due to a "separation bubble" forming immediately downstream of the turbulator which decreases heat transfer. Some of the results from the 50000 Reynolds number are shown in Figure 42 and Figure 43. As predictable, the Nusselt numbers for the 50000 conditions are significantly higher than the 25000. These trends of increasing Nusselt number with respect to Reynolds number are matched in this experiment, isothermal experiment, as well as the rotating section experiment. The turbulators in both Reynolds number experience increasing Nusselt number across the passage length due to the developing vortex. However, the smooth panel experiments are shown to be increasing in a similar nature. There is no explanation for this currently, however the RTV glue in the inlet is believed to have acted as a turbulator by clogging some of the inlet cross sectional area up. This would cause the smooth panel to behave like a turbulated panel. In addition, the flow in this experiment is developing whereas the rotating section has fully developed flow at the inlet. These boundary conditions will cause the Nusselt number to be higher in the developing flow experiment when compared to the fully developed flow experiment.

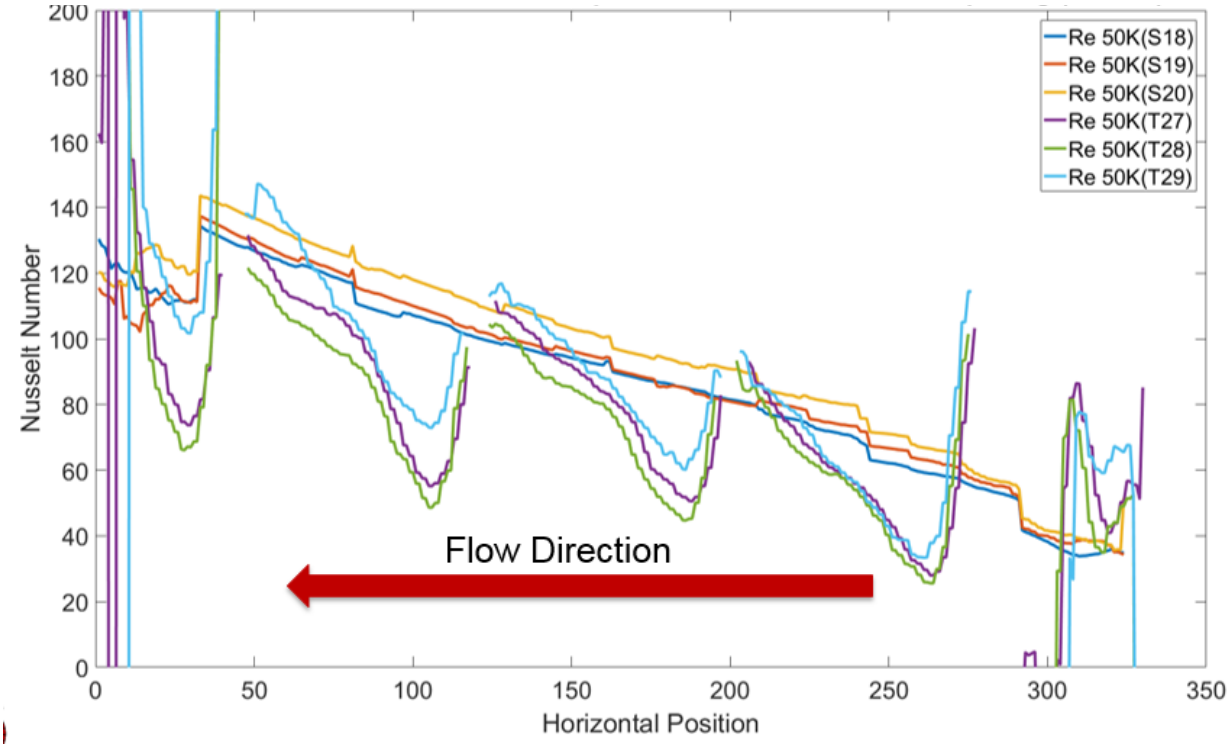

Figure 42. Turbulator vs Smooth Panel Nusselt Number Distribution Mid-Span 3.0 Seconds after Valve Opening at Reynolds 50000

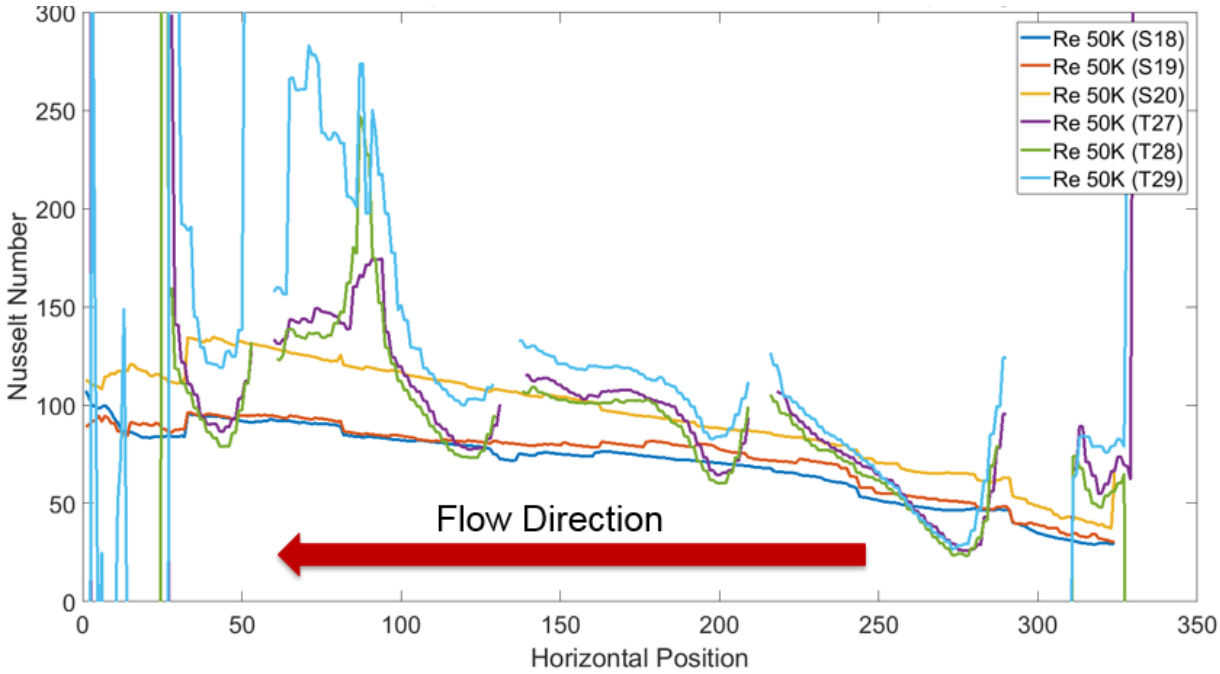

Figure 43. Turbulator vs Smooth Panel Nusselt Number Distribution 2/3 Span-Wise Distribution 3.0 Seconds after Opening of Valve

Additionally, to see the flow structure of the TLC experiments, a contour plot is created at Reynolds 25000 and 50000 1.5 seconds after valve is opened. These contour plots are seen in Figure 44. The flow structure can be observed to be similar in all cases. For the 25000 Reynolds case, the flow is seen to have the strongest vortex downstream of the 4th turbulator with a Nusselt number of approximately 100, and the same location in the Reynolds 50000 experiment experiences the strongest vortex resulting in a Nusselt number of approximately 200. As can be seen by the earlier span-wise distribution plots and the contour plots, the bottom span of the turbulated panel experiences the highest heat transfer.

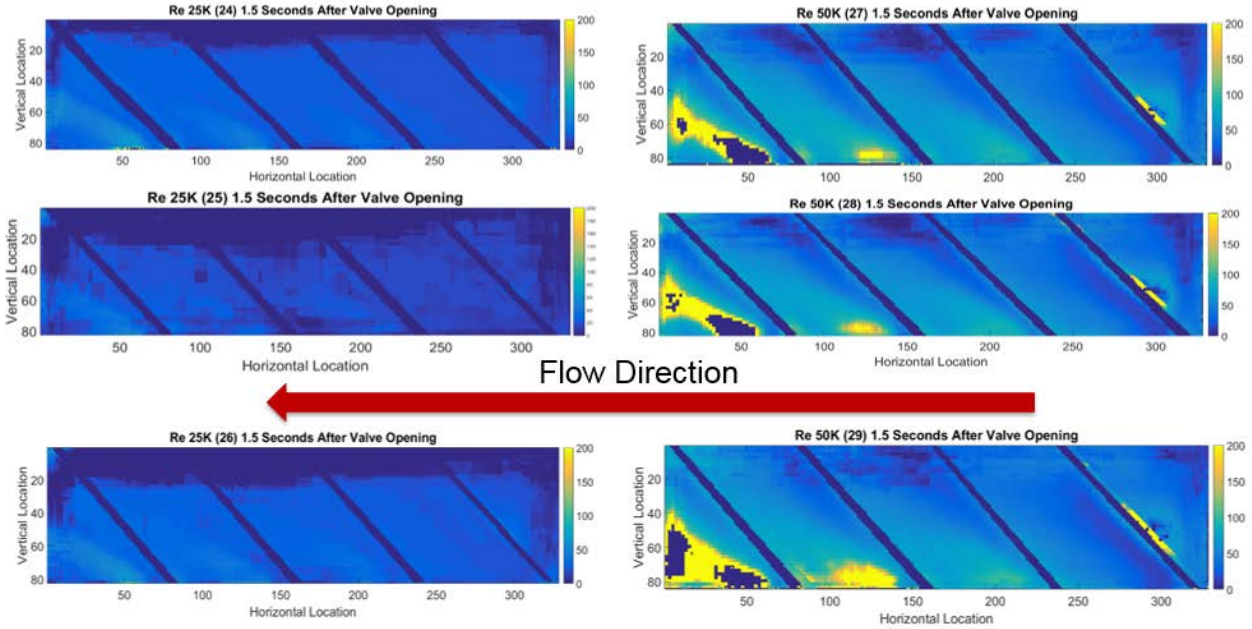

Figure 44. Contour Plots of Reynolds 25000 and 50000 Turbulated Panel 1.5 Seconds after Valve Opening

Chapter 4: Conclusion

This chapter outlines a few preliminary conclusions drawn from the experiment as well as providing a brief comparison to the single panel copper panel experiment being conducted by Howard at the GTL.

4.1 Conclusion

Throughout this study, the TLCs are observed to display higher Nusselt numbers at higher Reynolds number but considerably different Nusselt numbers when compared to the isothermal copper panel data. While comparing TLC results to themselves, it is clear that there is an error in the experiment which is resulting in higher Nusselt numbers for smooth panels. The immediate conclusion is that the RTV upstream of the inlet is acting like a turbulator, which is causing discrepancy within the result. Another possibility to investigate is the effect of sector calibrations. The sectors are causing discontinuities in wall temperature across the passage length that can contribute to stair-stepping Nusselt numbers. However, it is clear that there is a physical difference between the transient TLC experiment and the isothermal copper panel experiment. Shown in Figure 45 are results from Howard's copper panel experiment at same Reynolds numbers compared to the TLC single panel experiments from this project. As can be observed Nusselt number is consistently lower than the Copper Panel data, a trend also seen in the rotating section data. However, increasing the Reynolds number from 25000 to 50000 results in a Nusselt number increase of 50.7% for smooth copper panels. This same increase results in a 44.97% increase in TLCs. However, when keeping Reynolds number constant and changing geometry from smooth to turbulated, copper panel experiments result in a 61.2% increase in Nusselt number whereas the TLC results in a 24.0% increase.

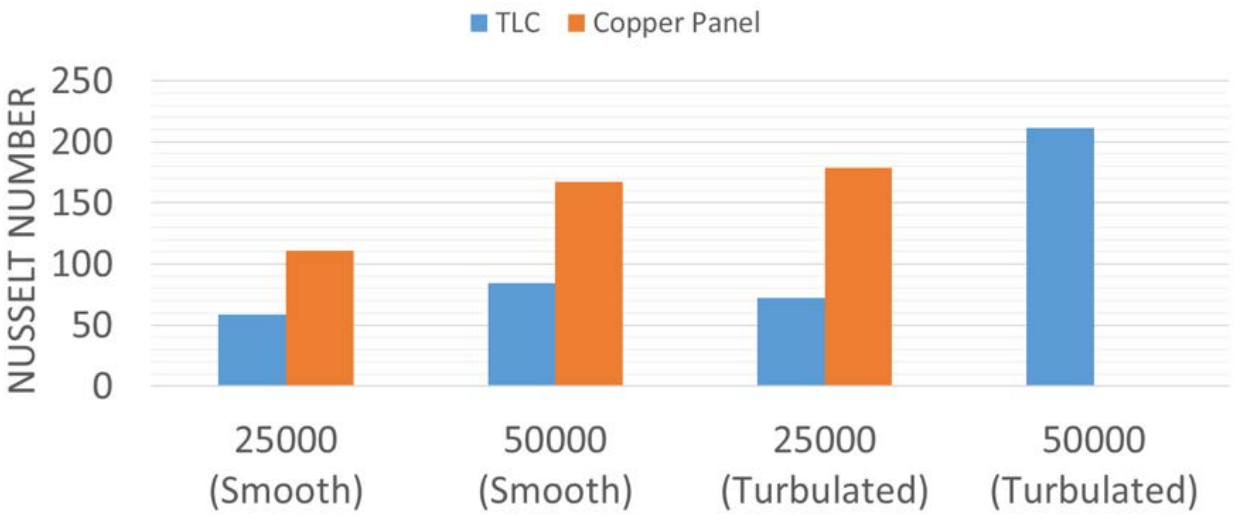

Figure 45. Comparison to Single Copper Panel Experiments at 25000 and 50000 Reynolds Number for Turbulated and Smooth Panel

4.2 Future Work

Some future steps to take for this project will be to clean up the inlet to ensure no RTV remains inside of the inlet and run multiple runs to check validity of smooth panel results. Additionally, post-processing of current runs will be repeated using one calibration equation instead of 18 to test effects of discontinuity on Nusselt number results for both smooth and turbulated panels. Future plans are being made to ensure the flow will be fully developed when entering the inlet for the panel to ensure a correct comparison to the rotating panel. Two methods of accomplishing this would be: increasing length of inlet pipe or increase inlet length with turbulators printed inside the area to trip the flow. On the computational side, a heat transfer model will be setup to investigate effectiveness of semi-infinite solid assumption for time window purposes for average Nusselt number calculations. The final step to take is to run copper panels at constant surface heat flux and detect temperature with an IR camera to change boundary condition and see the effect on Nusselt numbers.

Bibliography

Celestina, R., & Reagans, M. (2015). USER MANUAL: A User Guide and Manual for TLCcal.

Haldeman, C. (2006). *Conversion of Pyrex Heat-flux Sensor Data Reduction from a Relative Temperature to an Absolute Temperature Basis*.

Hay, J. L., & Hollingsworth, D. K. (1996). A comparison of trichromic systems for use in the calibration of polymer-dispersed thermochromic liquid crystals. *Experimental Thermal and Fluid Science*, *12*(1), 1–12. https://doi.org/10.1016/0894-1777(95)00013-5

Howard, R. (2017). *IHT Copper Plate Method [PowerPoint slides].*

Kakade, V. U., Lock, G. D., Wilson, M., Owen, J. M., & Mayhew, J. E. (2009). Accurate heat transfer measurements using thermochromic liquid crystal. Part 2: Application to a rotating disc. *International Journal of Heat and Fluid Flow*, *30*(5), 950–959. https://doi.org/10.1016/j.ijheatfluidflow.2009.04.005

Lawler, T. R. (2015). *Heat Transfer for a Stationary Serpentine Passage using a Transient Thermochromatic Liquid Crystal Pain Technique*. The Ohio State University.

Smith, M. A., Mathison, R. M., & Dunn, M. G. (2013). Heat Transfer for High Aspect Ratio Rectangular Channels in a Stationary Serpentine Passage With Turbulated and Smooth Surfaces. *Journal of Turbomachinery*, *136*(5), 51002. https://doi.org/10.1115/1.4025307

Stasiek, J. a, & Kowalewski, T. a. (2002). Thermochromic liquid crystals applied for heat transfer research. *Opto-Electronics Review*, *10*(1), 1–10. https://doi.org/10.1117/12.472179

You, R., Li, H., Wei, K., & Tao, Z. (2017). Two-dimensional heat transfer distribution in a rotating smooth rectangular channel with four surface heating boundary condition. *Advances in Mechanical Engineering*, *9*(10), 1–15. https://doi.org/10.1177/1687814017733243